Optimum Nusselt Number for Simultaneously Developing Internal Flow Under Conjugate Conditions in a Square Microchannel

Manoj Kumar Moharana

Piyush Kumar Singh

Sameer Khandekar[1]

e-mail: samkhan@iitk.ac.in

Department of Mechanical Engineering,
Indian Institute of Technology Kanpur,
Kanpur, UP 208016, India

A numerical study has been carried out to understand and highlight the effects of axial wall conduction in a conjugate heat transfer situation involving simultaneously developing laminar flow and heat transfer in a square microchannel with constant flux boundary condition imposed on bottom of the substrate wall. All the remaining walls of the substrate exposed to the surroundings are kept adiabatic. Simulations have been carried out for a wide range of substrate wall to fluid conductivity ratio ($k_{sf} \sim 0.17–703$), substrate thickness to channel depth ($\delta_{sf} \sim 1–24$), and flow rate ($Re \sim 100–1000$). These parametric variations cover the typical range of applications encountered in microfluids/microscale heat transfer domains. The results show that the conductivity ratio, k_{sf} is the key factor in affecting the extent of axial conduction on the heat transport characteristics at the fluid–solid interface. Higher k_{sf} leads to severe axial back conduction, thus decreasing the average Nusselt number ($\overline{Nu}$). Very low k_{sf} leads to a situation which is qualitatively similar to the case of zero-thickness substrate with constant heat flux applied to only one side, all the three remaining sides being kept adiabatic; this again leads to lower the average Nusselt number ($\overline{Nu}$). Between these two asymptotic limits of k_{sf}, it is shown that, all other parameters remaining the same (δ_{sf} and Re), there exists an optimum value of k_{sf} which maximizes the average Nusselt number ($\overline{Nu}$). Such a phenomenon also exists for the case of circular microtubes. [DOI: 10.1115/1.4006110]

Keywords: microchannel, axial heat conduction, conjugate heat transfer, thermally developing flow, optimum Nusselt number

1 Introduction

The last decade has witnessed rapid progress in the development of microchannel based thermofluidic systems. Enhanced species transport in such microgeometries is the prime motivation for their development. Applications of microgeometries, having characteristic dimensions ranging from a few micrometers to about 1000 μm, include electronics thermal management units, compact microheat exchangers, microscale chemical reactors, lab-on-chip devices, etc., to name a few [1–3]. On many instances, metals and alloys, silicon, or soft materials, e.g. Polydimethylsiloxane (PDMS), are used for fabrication of such devices, wherein circular or noncircular channels are fabricated in the form of an array [4–8]. It is also observed that the overall dimensions of the cross section of the substrate or the microchannel array (for example, the wall thickness, the interchannel pitch, the substrate thickness, etc.) frequently scales with the hydraulic diameter of the channel or duct used for fluid flow and heat transfer. Axial heat conduction along the solid walls of heat exchangers involving mini/microchannels are quiet often overlooked during the design/analysis stage and interpretation of experimental data to estimate the heat transfer coefficient. This frequently leads to erroneous conclusions and inconsistencies in interpretation of data. In reality, quite commonly, the apparently pure convective problem manifests itself in terms of conduction heat transfer in the substrate wall coupled with the convective heat transfer to or from the working fluid under consideration. The temperature and/or heat flux distribution at the conjugate wall(s) of the channel(s) depends on (a) thermal properties of the solid substrate and the fluid involved, (b) flow characteristics of fluid, and (c) dimensions of the solid and fluid domain, respectively. In real-time situations, it becomes imperative to apply the boundary condition(s) at a certain finite distance from the fluid–solid interface. The resulting conjugate nature of heat transfer leads to the distortion of the actual boundary condition at the fluid–solid interface. The order of magnitude of this distortion is naturally more in regions where large temperature gradients exist, for example, in the thermal entrance region of a heated duct.

In the context of laminar duct flow in microchannels, conjugate heat transfer leads to a strong multidimensional coupling. The small dimensions of microchannels in the transverse direction are often comparable to the substrate thickness. As the hydraulic diameter of microchannels decreases, this coupling between the substrate and bulk fluid temperatures becomes significant. It is important to explicitly identify the thermofluidic parameters of interest which lead to a distortion in the boundary conditions and thus the true estimation of species transfer coefficients. To quantify the effect of axial conduction in the substrate on internal single-phase convective flows, the concept of "conduction parameter," a quantity that gives relative importance of conduction heat transfer compared to the energy flow carried by the fluid, exists in the literature from some time. It is defined as the ratio of axial heat transfer within the solid duct or tube due to axial temperature gradient in it to the energy flow carried by the fluid in the channel in the axial direction. This parameter was used by Bahnke and Howard [9] for analysis of recuperators, and in later years, by

[1]Corresponding author.

Contributed by the Heat Transfer Division of ASME for publication in the JOURNAL OF HEAT TRANSFER. Manuscript received May 26, 2011; final manuscript received December 20, 2011; published online May 22, 2012. Assoc. Editor: Kenneth Goodson.

Peterson [10,11] for conduction effects in microscale counter-flow heat exchangers. It is defined as

$$\lambda = (k_s \cdot A_s)/(\dot{m} \cdot c_p \cdot L) \tag{1}$$

where the average mass flow rate is $\dot{m} = \rho_f \cdot A_f \cdot \bar{u}$.

The physical interpretation of the effects due to axial conduction in the substrate can be studied by considering the three natural nondimensional parameters of this problem, i.e., (i) Number of transfer units of the system, NTU, (ii) Biot number, defined on the basis of the thickness of the substrate, and (iii) the wall size ratio, defined as

$$\mathrm{NTU} = \frac{h \cdot L}{\rho_f \cdot c_{p-f} \cdot \delta_f \cdot u}, \quad \mathrm{Bi} = \frac{h \cdot \delta_s}{k_s}, \quad \text{and} \quad \xi = \frac{\delta_s}{L} \tag{2}$$

By considering these three nondimensional parameters, Maranzana et al. [12] reintroduced the same concept of λ and named it as "axial conduction number (M)," defined as the ratio of the conductive heat flux to the convective counterpart

$$M = \frac{\dot{q}'_{cond\|}}{\dot{q}'_{conv}} = \left(k_s \frac{(\delta_s \cdot \omega)/L}{(\rho_f \cdot c_{p-f} \cdot \delta_f \cdot \omega \cdot \bar{u})} \right) = \frac{\xi^2 \cdot \mathrm{NTU}}{\mathrm{Bi}} \tag{3}$$

Here, $\dot{q}'_{cond\|}$ gives the first order estimation of the axial heat flux in the wall, assuming the transfer is one-dimensional along the length of the channel, through the same temperature difference which the fluid experiences between channel inlet and outlet. As will be appreciated, this number M is usually very low in macrochannels due to the low ratio of solid to fluid domain thickness (δ_{sf}), higher flow velocity, and longer channel length. This implies that conductive heat transfer in solid walls of conventional macrosized ducts is nearly one-dimensional and perpendicular to the fluid flow. This is usually not the case when the size of the channels decreases to micro or smaller ranges. Maranzana et al. [12] carried out analytical study as well as numerical simulation to understand axial heat conduction phenomena in a mini/micro counter-flow heat exchanger. Based on their analysis, they stated that the effect of axial conduction in the substrate on the heat transfer coefficient can be neglected if $M < 10^{-2}$.

Both the conduction parameter (λ) and the axial conduction number (M) are based on the assumption that the axial temperature difference between the inlet and outlet location in the solid substrate (ΔT_s) as well as in fluid (ΔT_f) domain is same; this assumption is rather unrealistic though. To address this shortcoming in the definition of parameter M (or λ), as defined by Maranzana et al. [12], Li et al. [13], and later Zhang et al. [14] incorporated the effect of individual temperature differences between the inlet and outlet location in the solid substrate (ΔT_s) as well as in fluid (ΔT_f) domain. The conduction number, as revised by Li et al. [13], is given by

$$M = \frac{k_s}{\rho_f c_p \bar{u} L} \frac{A_s}{A_f} \frac{\Delta T_s}{\Delta T_f} \tag{4}$$

where ΔT_s and ΔT_f are the difference in average temperature of the cross section at inlet and outlet of solid and fluid region, respectively.

Based on the outcome of numerical investigations, Zhang et al. [14] stated that the criteria ($M < 10^{-2}$) proposed by Maranzana et al. [12] is not always valid.[2] They highlighted that the criteria for judging the effect of axial heat conduction in the substrate wall may be situation or problem dependent. They highlighted that there was considerable effect of wall axial heat conduction in the circular tube considered by them in spite of the fact that the parameter M was less than 10^{-2}. It was also pointed out that the criteria proposed by Maranzana et al. [12] is not suitable for the analysis of thermally developing fluid flow and heat transfer in microchannels.

Conjugate problems have been studied long before the development of micro heat exchangers. Petukhov [15] proposed the following parameter to characterize the effect of axial conduction in a circular tube

$$P = k_{sf} \cdot \left[1 - (1 + (\delta/r_i))^2 \right] \tag{5}$$

where δ is the wall thickness, r_i is the inner radius, and k_{sf} is the ratio of conductivity of solid (circular tube) to the conductivity of the fluid flowing inside it. Several other criteria to judge the influence of wall heat conduction on the duct/passage flow convection have also been proposed as indicated by Lelea [16]. In the context of a circular tube, Faghri and Sparrow [17] indicated that wall conduction parameter is a measure of the strength of axial conduction in its wall, and defined it as

$$P = k_{sf}(\delta/r_i) \tag{6}$$

The correlation by Cotton and Jackson [18] is of the form

$$P = k_{sf} \left[\frac{\delta}{d_i} \left(1 + \frac{\delta}{d_i} \right) \right] \left(\frac{1}{Pe^2} \right) \tag{7}$$

and the correlation by Chiou [19] is given by

$$P = k_{sf} \cdot A_{sf} \cdot (d_i/L) \cdot (1/Pe) \tag{8}$$

As indicated in Hessel et al. [20], if the conduction parameter defined by Chiou [19] in Eq. (8) is less than 0.005, the axial heat transfer through conduction in the channel wall can be neglected.

Recently, Cole and Cetin [21] reported analytical solution for conjugate heat transfer in a parallel-plate microchannel using Green's functions. They reported that axial conduction in the channel wall is important under the following conditions: (a) length over height ratio of the microchannel is very small, (b) Peclet number is very small, (c) wall thickness relative to the channel height is large, and (d) conductivity of wall material is high relative to conductivity of the fluid.

Although a number of numerical [4,5,8,13,14,22–25] and experimental [6,8,13,22,26,27] studies have been performed on the effect of wall heat conduction on hydrodynamically and/or thermally developing flows in mini/microchannel and tubes, an explicit discerning parameter for judging the effect of axial conduction in the substrate on the local and average Nusselt number in the entry length is not available. Sufficient number of parametric studies is also not readily available; most reported studies deal with only circular microtubes. Rectangular microchannels are of particular interest as they are used extensively as heat sinks in microelectronic devices, as well as for catalytic reactors for micro fuel processors, biological sensors, etc. [28,29]. Such rectangular mini/microchannels are often employed in high heat flux dissipating heat exchanger equipment. In most devices or systems, the location of application of the boundary condition is somewhat away from the actual fluid–solid boundary. Moreover, depending on the application, the material used for manufacturing the substrates may have a wide range of thermal conductivities. The aspect ratio of the channel and the overall substrate dimensions is also chosen as per the need in a given application. For the estimation of realistic heat transfer coefficients for such wide-ranging design parameters, especially under simultaneously developing flow regime wherein the heat transfer coefficients are high, and therefore of interest, the importance of a thorough parametric study to discern the magnitude of axial conduction affecting the heat transport coefficient, cannot be overemphasized. This is the

[2]It is to be noted here that Zhang et al. [14] used the axial conduction number as revised by Li et al. [13], i.e., Eq. (4).

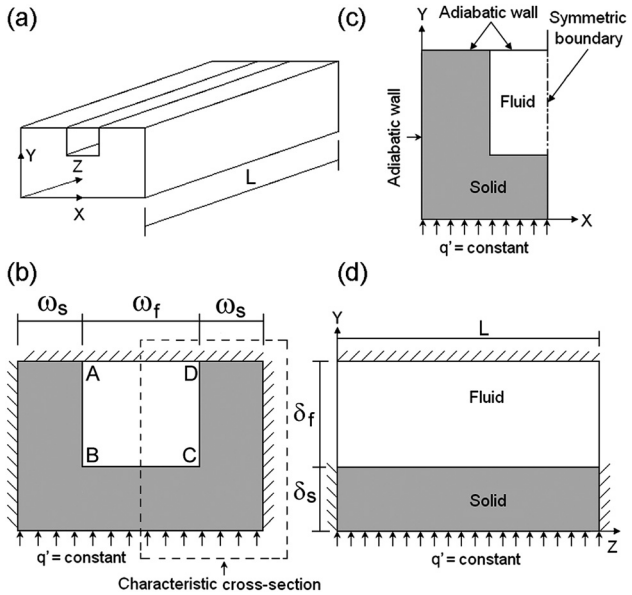

Fig. 1 Details of the simulated domain: (*a*) Microchannel with conductive wall, (*b*) channel cross section, (*c*) the computational domain (chosen from symmetry conditions), and (*d*) transverse section (Y-Z) plane along the plane of symmetry

aim of the present numerical study, which focuses on simultaneously developing laminar flow and heat transfer in a square duct with constant heat flux applied at the bottom of the substrate. The conductivity ratio (k_{sf}) has been varied from 0.17 to 703 (to cover a wide range of materials) while the bottom wall thickness to channel height ratio (δ_{sf}) ranges from 1 to 24. The flow Reynolds number has been varied from 100 to 1000. All other parameters remaining the same, it has been observed that average Nusselt number $\overline{Nu}$, for simultaneously developing laminar flow under conjugate conditions, exhibits maxima with respect to the thermal conductivity ratio (k_{sf}) due to the effect of axial conduction in the substrate. The location of this maximum Nusselt number is a weak function of flow Reynolds number and the ratio δ_{sf}.

2 Numerical Analysis

We model simultaneously developing (slug flow inlet ($\bar{u}$)) single-phase, steady-state laminar incompressible flow with constant thermophysical properties (for both solid and liquid) in a microchannel geometry as schematically shown in Fig. 1(*a*). All the surfaces of the substrate exposed to the surrounding are assumed to be insulated, except the bottom surface where constant heat flux (q') boundary condition, simulating the heat generation, e.g., from an electronic chip, is specified. Only one half of the microchannel was included in the computational domain, in view of the symmetry conditions; this was also computationally efficient.

The dimensions of the substrate considered in the analysis are listed in Table 1. The width (ω_f), height (δ_f), and length (L) of the channel in the computational model are kept constant at 0.4 mm, 0.4 mm, and 120 mm, respectively. Thus, the hydraulic diameter (D_h) of the channel is 0.4 mm. While the width of the substrate ($2\omega_s + \omega_f$) is kept constant, the thickness of the substrate ($\delta_s + \delta_f$) is varied to understand the effect of its bottom wall thickness (δ_s) on the conjugate heat transfer behavior. This is because as the thickness of the substrate increases, the boundary on which constant heat flux is applied moves away from the actual solid–liquid interface.

Table 1 Dimensions of the microchannel substrate investigated ($\omega_f = \delta_f = 0.4$ mm)

ω_s (mm)	δ_s (mm)	L (mm)	δ_{sf}	Mesh (half domain)
0.4	0.4	120	1	$60 \times 80 \times 400$
0.4	0.8	120	2	$60 \times 120 \times 400$
0.4	3.2	120	8	$60 \times 360 \times 400$
0.4	6.4	120	16	$60 \times 680 \times 400$
0.4	9.6	120	24	$60 \times 1000 \times 400$

The associated species conservation equations for the fluid and the solid domain, i.e., the continuity, Navier–Stokes and the energy equation, along with the associated boundary conditions, for the conjugate problem, are as follows:

For the liquid domain

$$\nabla \cdot \vec{u} = 0 \tag{9}$$

$$\vec{u} \cdot \nabla \vec{u} = -\frac{1}{\rho}\nabla p + \frac{\mu}{\rho}\nabla^2 \vec{u} \tag{10}$$

$$\vec{u} \cdot \nabla T = (k/\rho \cdot C_p) \cdot \nabla^2 T \tag{11}$$

For the solid domain

$$\nabla^2 T = 0 \tag{12}$$

The applicable boundary conditions are

$$(\partial T/\partial x) = 0; \quad \text{Y-Z plane at } x = 0 \text{ and } x = (2\omega_s + \omega_f) \tag{13a}$$

$$(\partial T/\partial y) = 0; \quad \text{X-Z plane at } y = (\delta_s + \delta_f) \tag{13b}$$

$$(\partial T/\partial z) = 0; \quad \text{X-Y plane at } z = 0 \text{ and } z = L \tag{13c}$$

$$u = \bar{u}; \quad \text{X-Y plane at } z = 0 \tag{13d}$$

$$u = 0; \quad \text{no slip at all fluid-solid interfaces} \tag{13e}$$

A constant heat flux (q') is applied to the bottom of the substrate as typically encountered in many practical applications

$$q' = \text{constant}; \quad \text{X-Z plane at } y = 0 \tag{13f}$$

Peclet numbers considered in this work are large enough to assume that the axial conduction in the fluid domain will be negligible, as compared to that of the solid substrate [3]. Second, the work by Xu et al. [30], Koo and Kleinstreuer [31], and Morini [32], clearly suggest that viscous dissipation in the liquid can also be neglected for the range of parameters considered in this study. Working fluid (pure water) enters the microchannels with a slug velocity profile ($\bar{u}$) at an inlet temperature of 300 K. Above set of equations and the associated conditions are solved using the commercially available software ANSYS-FLUENT® [33]. The "standard scheme" was used for pressure discretization. The SIMPLE algorithm was used for velocity-pressure coupling in the multigrid solution procedure. The momentum and energy equations were solved using the second order upwind scheme. The entire domain was meshed using hexahedral elements and grid independence was ensured before the final grid size was chosen. For postprocessing of the data, the following nondimensional variables are used in this study:

$$\phi = \frac{\overline{q'_z}}{q'}, \quad \delta_{sf} = \frac{\delta_s}{\delta_f}, \quad z^* = \frac{z}{Re\,Pr\,D_h}, \quad Nu_z = \frac{h_z D_h}{k_f},$$
$$\Theta = \frac{T - T_i}{T_o - T_i}, \quad \Theta_f = \frac{T_f|_z - T_{fi}}{T_{fo} - T_{fi}}, \quad \Theta_w = \frac{T_w|_z - T_{fi}}{T_{fo} - T_{fi}} \tag{14}$$

where T_i and T_o are temperature of bulk fluid at location $z = 0$ (inlet), and $z = L$ (outlet), respectively. $\overline{q'_z}$ is the local heat flux at any axial

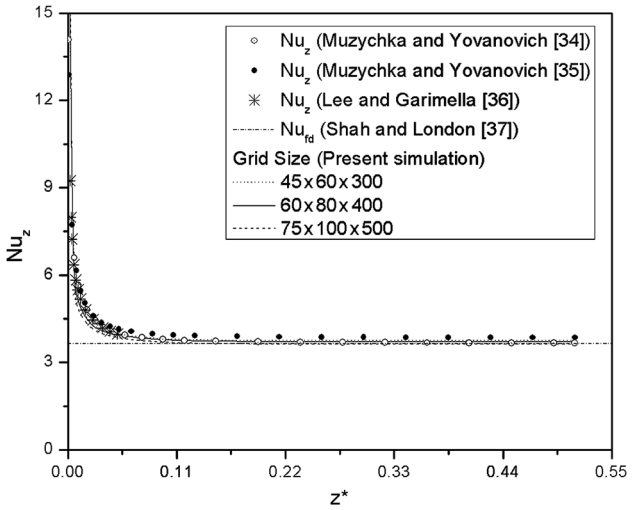

Fig. 2 Local Nusselt number as a function of dimensionless axial distance for different grids used to establish grid independence at $\delta_{sf} = 1$ and Re = 100

location z^* which is calculated by peripheral average of heat flux along the three conjugate walls (AB, BC, and CD in Fig. 1(*b*)) at the X-Y plane at that location, $\overline{q'}$ is the ratio of the applied heat power at the bottom of the substrate and the net area of the conjugate walls, i.e., total area of the fluid–solid interface, given by

$$\overline{q'} = (q') \cdot (2\omega_s + \omega_f)/(2\delta_f + \omega_f) \tag{15}$$

The Reynolds number is given by $Re = \rho \cdot \bar{u} \cdot D_h/\mu$ and the peripheral average local heat transfer coefficient is denoted by h_z. The local values h_z and $T_w|_z$ are calculated by performing peripheral averaging along the three conjugate walls (AB, BC, and CD in Fig. 1) of the channel, at the particular location of interest. The local fluid temperature, $T_f|_z$ is the channel cross-sectional area average bulk fluid temperature at any location z. Further, the average Nusselt number over the channel length is given by

$$\overline{Nu} = \int_0^L Nu_z dz \tag{16}$$

2.1 Grid Independence Check. Grid independence tests were conducted for all the geometries tested. As an example, local Nusselt number obtained for a substrate with $\delta_{sf} = 1$ for three different grids of $45 \times 60 \times 300$, $60 \times 80 \times 400$, and $75 \times 100 \times 500$, for Re = 100, is shown in Fig. 2. The local Nusselt number at the fully developed flow regime (at $z^* = 0.42$) changed by 1.06% from the grid size of $45 \times 60 \times 300$ to $60 \times 80 \times 400$ and changed by less than 1% upon further refinement to grid size of $75 \times 100 \times 500$. Since no appreciable change is observed as we moved from first to the third grid, the intermediate grid size of $(60 \times 80 \times 400)$ was chosen. All other cases were also individually tested for grid independence as described here and the most appropriate grid was chosen. Benchmark results from developing [34–36] as well as fully developed flow [37] with constant heat flux applied at the fluid–solid interface, were also verified before taking up the conjugate problem, as highlighted in Fig. 2.

3 Results and Discussion

As noted earlier, while the width of the substrate is kept constant, the thickness of the substrate in the Y direction is varied to understand the effect of substrate thickness on the heat transfer behavior. As the thickness of the substrate increases, the boundary on which constant heat flux is applied moves away from the actual fluid–solid interface, i.e., for the present case, the three sides of the channel. There is a basic difference between a circular duct (which was studied by Zhang et al. [14]) and a square duct in a substrate, as has been considered in the present study. In a circular duct, the fluid–solid interface always remains parallel to the outer duct surface on which constant heat flux is applied, whereas in the present case, while only one duct wall is parallel to the base of the substrate on which constant heat flux is applied, the remaining two conjugate walls are perpendicular to it. This makes the heat transfer in transverse direction a two-dimensional issue, unlike the case of circular tube/duct. Maximum heat transfer coefficient will occur if constant heat flux is experienced at the fluid–solid interface walls of the channel. As the actual location of constant heat flux is away from the fluid–solid interface, there will be a distortion of the boundary condition, and therefore the effective local heat transfer coefficient will change. The parameters which will discern the effect of axial conduction in the substrate, and therefore an alteration in the actual boundary condition, are the axial variation of average bulk fluid temperature, average local heat flux, and average wall temperature of the channel.

Figures 3–5, respectively, highlight the axial variation of dimensionless heat flux, dimensionless average wall and bulk fluid temperature, and local Nusselt number in the channel, under the parametric variation of thermal conductivity ratio (k_{sf}), thickness ratio (δ_{sf}), Reynolds number (Re), as collated in Table 2.

It is evident that the heat transfer process from the substrate to the fluid flowing in the channel is governed by the boundary condition experienced at the conjugate walls of the channel. Therefore, to find the actual value of heat flux experienced at the fluid–solid interface of the square channel, the axial variation of dimensionless local heat flux ϕ (averaged over the duct periphery) at the fluid–solid interface is presented in Fig. 3, for selected range of parameters from Table 2. It is clearly evident that the actual heat flux experienced at the fluid–solid interface is approximately axially uniform/constant at low conductivity ratio (k_{sf}) irrespective of the thickness ratio (δ_{sf}). At higher conductivity ratio (k_{sf}), the actual heat flux experienced at the fluid–solid interface deviates from the constant value applied at the bottom, with increasing thickness ratio (δ_{sf}). At very low thickness ratio (δ_{sf}), the actual heat flux experienced at the fluid–solid interface is equal to the actual value of heat flux applied at the bottom of the substrate except at the region very near to the inlet, where developing thermal boundary layer dominates. This qualitative pattern of axial variation in local heat flux is due to the fact that low thermal conductivity ratio leads to higher axial thermal resistance in the substrate and vice versa. Accordingly, at higher k_{sf}, low axial thermal resistance of the substrate leads to significant back conduction; this effect becomes naturally more prominent with increase in thickness ratio δ_{sf}. It can be observed that for higher k_{sf} and δ_{sf} (in Fig. 3(*a*)) the boundary condition at the fluid–solid interface increasingly approach the trend closer to an isothermal temperature boundary condition, although constant heat flux was applied at the bottom of the substrate. Analogous observations were reported by Zhang et al. [14] who applied a constant temperature boundary condition at the outer surface of a circular tube and found that the dimensionless heat flux at the fluid–solid boundary tends to become constant when axial conduction in the tube wall dominates.

The axial variations of dimensionless wall temperature Θ_w (averaged over the periphery of the channel wall) as well as the bulk fluid temperature Θ_f are presented in Fig. 4 for Re = 100, 500, 1000 and $k_{sf} = 0.8$, 26, and 635. At low conductivity ratio k_{sf}, irrespective of the thickness ratio (δ_{sf}), the wall and the fluid temperatures rise as per the conventional theory applicable for ducts with zero wall thickness. In such cases, after the flow has

Table 2 Range of parameters considered for simulations

Re	k_{sf}	δ_{sf}	Pr
100, 500, 1000	0.17–703.0	1, 2, 8, 16, 24	5.85

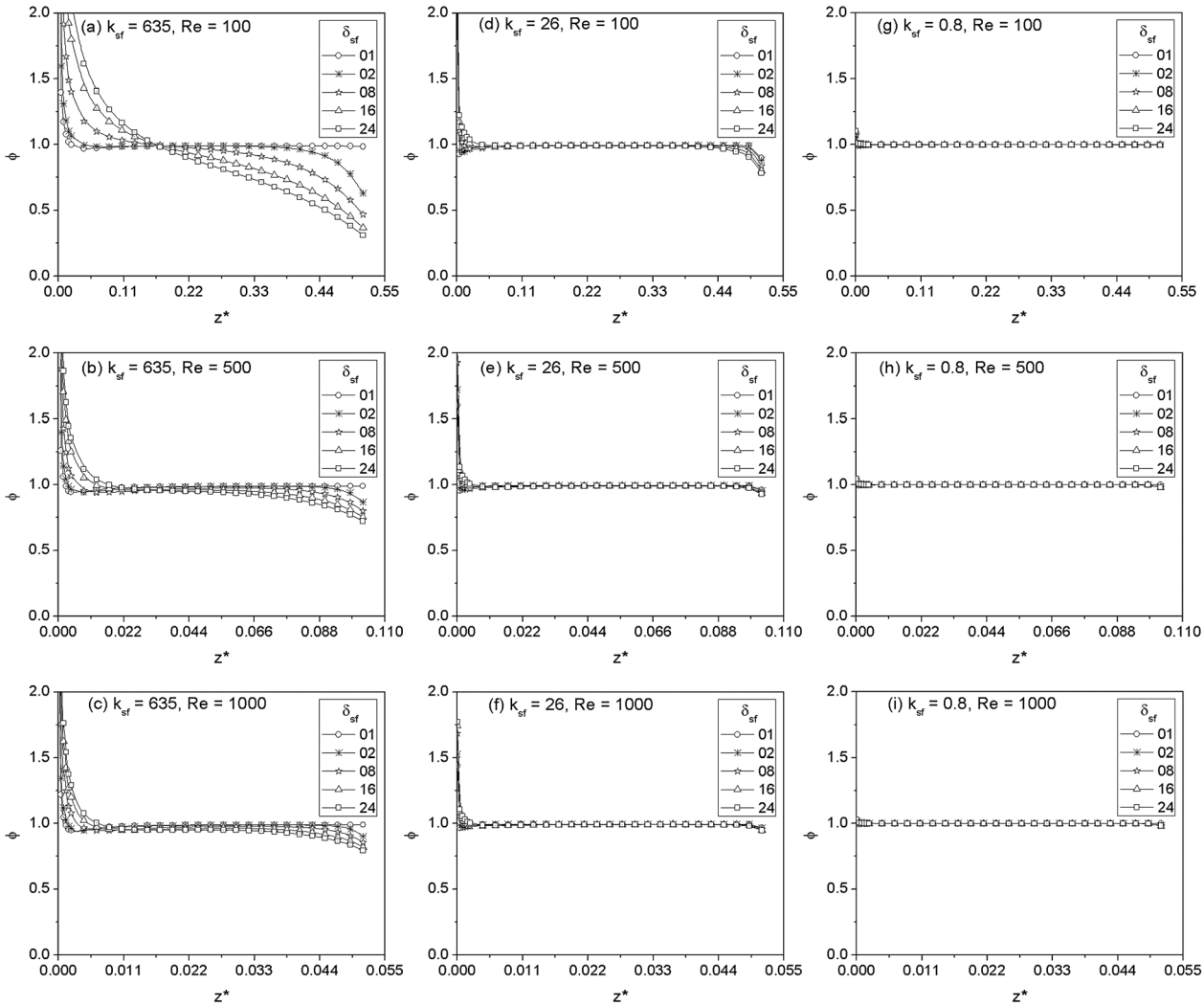

Fig. 3 Axial variation of dimensionless local surface heat flux at the fluid–solid interface

fully developed, the temperature difference $(\Theta_w - \Theta_f)$ attains a constant value. In contrast, as the conductivity ratio k_{sf} increases, there is a clear deviation in the "well ordered" behavior of the wall and the fluid temperature. The fluid temperature rise is no longer linear indicating that the condition of constant heat flux boundary is being compromised due to the conjugate nature of heat transfer in the substrate. The wall temperature variation clearly indicates heat flow from the downstream location of the substrate toward the upstream direction. This tends to "isothermalize" the wall temperature on the fluid–solid boundary. This is also reflected in the gradual occurrence of exponential component superimposed on the linear fluid temperature profile, indicative of a shift toward a pseudo-constant temperature boundary condition experienced by the fluid at the boundary interface. This effect is clearly more prominent as the thickness ratio δ_{sf} goes on increasing; this further increases the thermal resistance offered by the substrate, manifesting the conjugate nature of heat transfer.

The ensuing axial variation of local Nusselt number (Nu_z) is represented in Fig. 5. This figure corresponds to the results of Figs. 3 and 4, discussed earlier. Two dotted lines indicate the two respective asymptotic Nusselt number values for fully developed flow, without any conjugate heat transfer (i.e., wall thickness = 0) in: (i) a square channel heated from three sides and insulated from the fourth side; for this case the Nu = 3.556 and (ii) a square channel heated from one side, three remaining sides being insulated; for this case the Nu = 2.712 [37]. It is clearly observable from Fig. 5 that for substrates with conductivity ratio $k_{sf} = 26$, the value of Nu_z is independent of thickness ratio (δ_{sf}) and converges to a value of about 3.556 in the fully developed region, as expected. For substrates with very high conductivity ratio (i.e., $k_{sf} = 635$) and very low thickness ratio ($\delta_{sf} = 1$), the value of Nu also converges to a value which is more or less equal to 3.556. As the substrate thickness ratio (δ_{sf}) is increased, the value of Nu for thermally developed region decreases and drifts away from the value of 3.556. This can be explained in the background of the fact that, as explained earlier for these cases in Figs. 3 and 4, the boundary condition at the fluid–solid interface gets distorted due to conjugate effects; it tends to be experienced as a "pseudo-isothermal" boundary condition by the convective fluid. This is due to axial back conduction, as was also observed in Fig. 3 and 4. For substrates with exceedingly low conductivity ratio ($\sim k_{sf} = 0.8$), the value of Nu_z converges to 2.712, suggesting that under such a situation, the heat transfer takes place predominantly through the bottom channel wall, leading to the asymptotic behavior, inline with the data suggested in Shah and London [37] for a channel with only one side heating and the rest three sides being insulated.

For the purpose of benchmarking, Fig. 5 also depicts Nu_z estimates for two more reference cases, which are not exactly as the present case under study, nevertheless are similar in some respects:

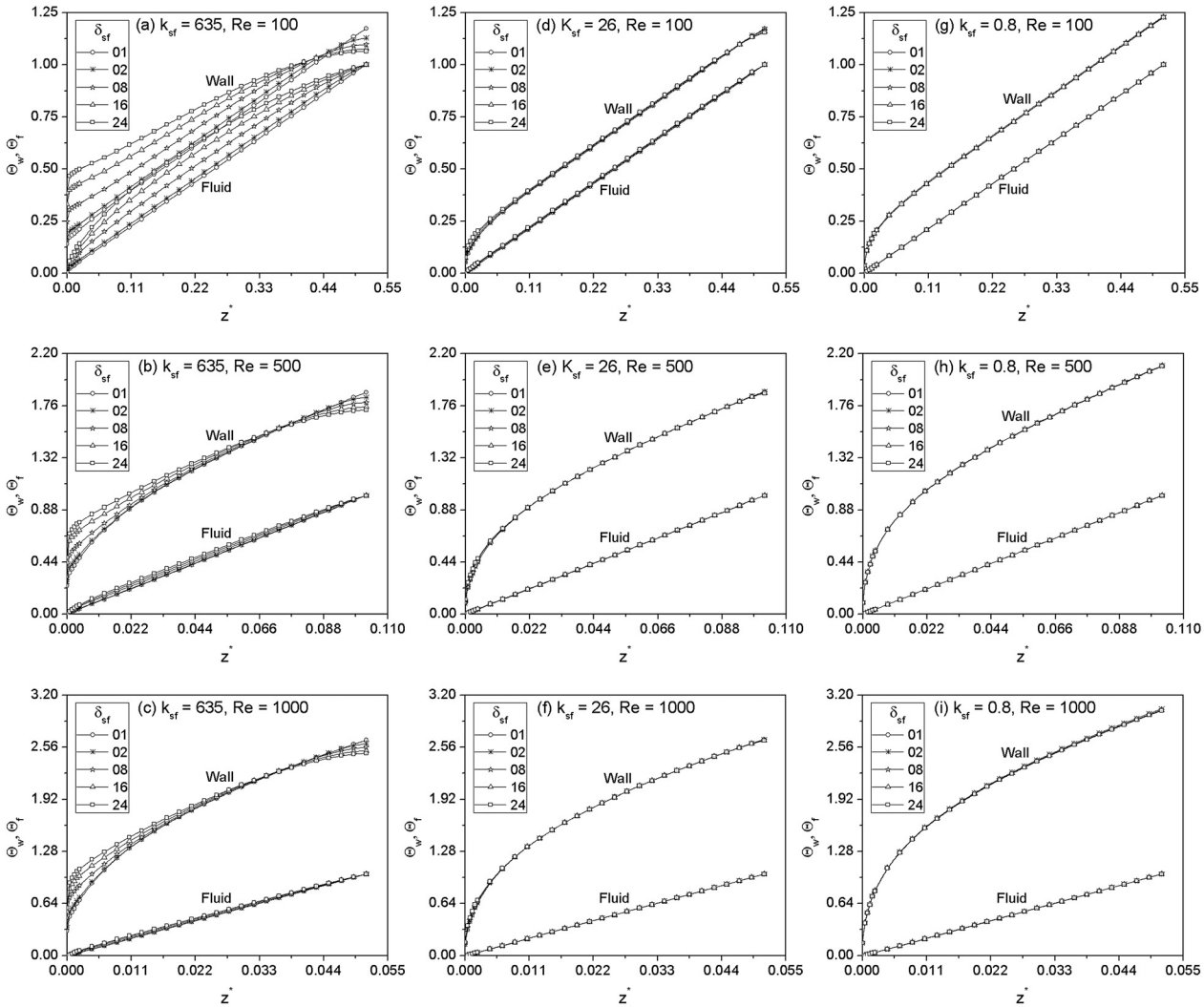

Fig. 4 Axial variation of dimensionless peripheral averaged local wall temperature and bulk fluid temperature

Case 1: Correlation developed by Lee and Garimella [36], for hydrodynamically fully developed but thermally developing flows (This correlation is valid in the thermally developing zone only).

Case 2: Data for simultaneously developing laminar flow in a square channel for a fluid having $Pr = 0.7$, as reported in Shah and London [37]. For simultaneously developing flows, dependency of Nusselt number on Prandtl number is much stronger [37]. For the present study, since $Pr = 5.85$, Nu_z is always smaller than this reference case having $Pr = 0.7$, as expected for a simultaneously developing flow.

From Fig. 5, it can also be concluded that the dominance of the ratio k_{sf}, in affecting the alteration in the local Nusselt number due to conjugate heat transfer effects, is higher than the geometric ratio δ_{sf}. Second, one of the important findings is that while a higher value of k_{sf} increases the effect of axial conduction in the substrate thereby lowering the Nusselt number, a lower value of k_{sf} tends to fundamentally alter the spatial distribution of heat as it gets transferred to the fluid through the three walls of the channel, which, in turn, again lowers the effective local Nusselt number. Thus, it is logically expected that an optimum k_{sf} for maximizing the Nusselt number exists, in-between these two asymptotic transport mechanisms, which leads us to Fig. 6, wherein the variation of average axial Nusselt number ($\overline{Nu}$) as a function of conductivity ratio (k_{sf}), while parametrically varying the flow Re and δ_{sf}, has been plotted. The occurrence of the optimum k_{sf} for maximizing the average Nusselt number is clearly exemplified here.

At $k_{sf} = 0$, the $\overline{Nu}$ will obviously be zero, irrespective of substrate thickness, as the substrate just does not conduct any heat through it. As k_{sf} increases to a vanishingly small value, heat flow commences and $\overline{Nu}$ sharply increases; this is observed for the entire range of flow Re and δ_{sf}. After attaining a maximum value, $\overline{Nu}$ again shows a downward trend with increasing k_{sf}, although the downward slope of this decrease in $\overline{Nu}$ is comparatively rather moderate. This decrease in $\overline{Nu}$ is primarily due to the increasing effects of conjugate heat transfer in the substrate, leading to axial back conduction of heat. The simulations suggest that the k_{sf} corresponding to the maximum $\overline{Nu}$ is a function of both, the flow Re and δ_{sf}, although the dependence on the latter is not very strong. For a given flow Re, the importance of k_{sf} as the dominating parameter in affecting the maximum $\overline{Nu}$, as compared to the geometric parameter δ_{sf}, is also quite obvious from these simulations. From Fig. 6, it can also be observed, inline with conventional observation for developing flows, that the average Nusselt number value, for a given geometry and conductivity ratio, increases with increasing flow Re.

To understand the effect of conductivity ratio more clearly, the peripheral variation of dimensionless heat flux passing through the fluid–solid interface is shown in Fig. 7(*a*) and 7(*b*) for different values of k_{sf}, at $Re = 100$ and $\delta_{sf} = 1$ and 16, respectively, on the X-Y plane at halfway through the length of the channel. For lower values of k_{sf}, the boundary condition at the fluid–solid interface changes substantially. With decreasing k_{sf}, the heat flux

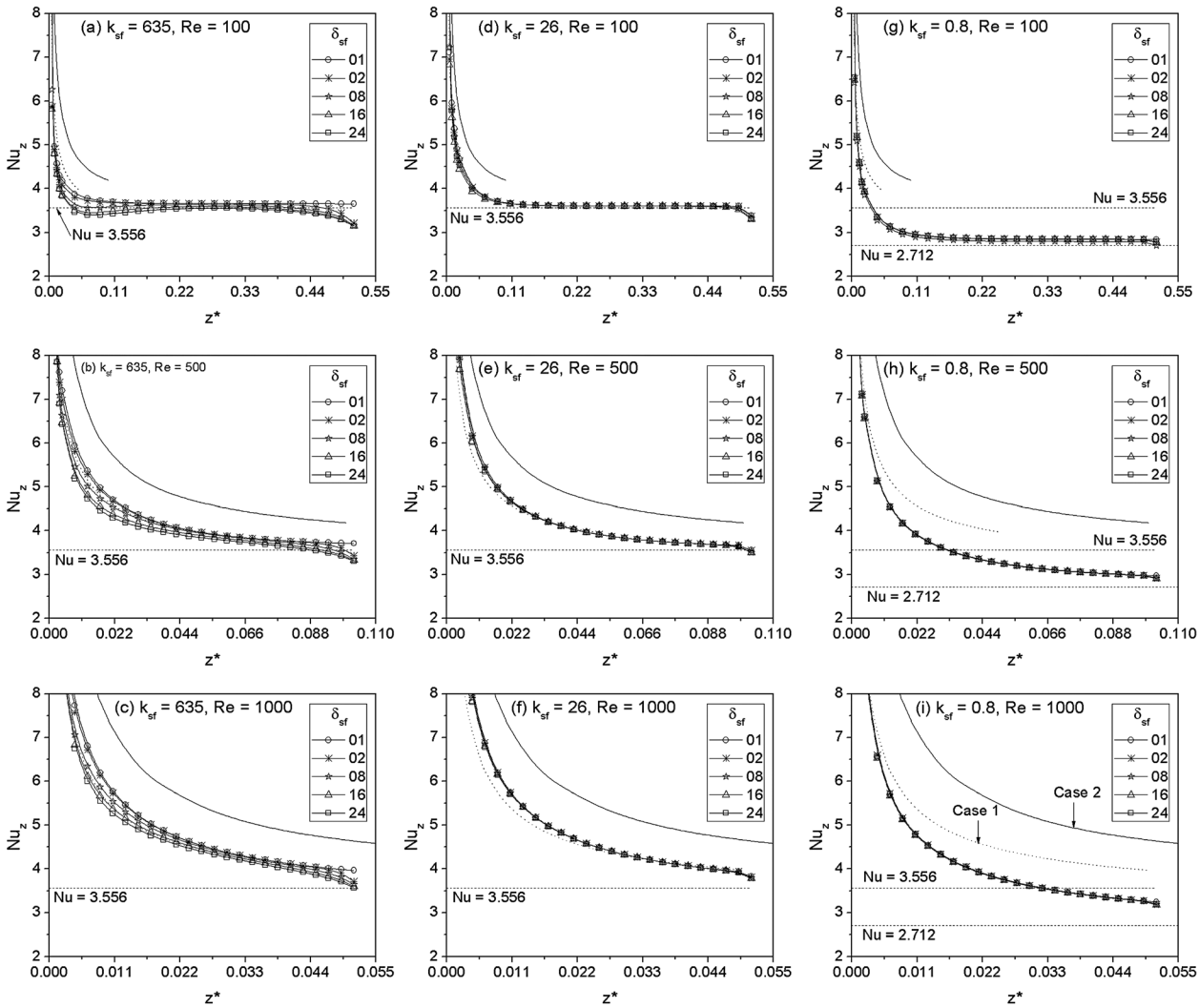

Fig. 5 Axial variation of local Nusselt number, Nu_z, for the range of simulation parameters

through the vertical interfaces (AB and CD; see inset in Fig. 7(*a*) and 7(*b*)) decreases and the heat flux through the horizontal interface (BC) increases; shifting the situation closer to one side heating rather than three side heating of the channel. Under such a situation, the thermal resistance for heat flow through the vertical interfaces, AB and CD, is quite high as compared to that of the horizontal interface, BC. In contrast, at very high conductivity, the thermal resistance to heat flow through the vertical interfaces decreases considerably, thereby manifests the heat flux distribution, as shown on Fig. 7. In addition, increasing the thermal conductivity ratio also decreases the thermal resistance in the longitudinal direction, along the flow, leading to axial back conduction; this combined effect causes $\overline{Nu}$ to again decrease with increasing k_{sf}. Figure 7(*b*) shows that qualitatively there is little difference in the behavior of $\overline{Nu}$, if the thickness ratio δ_{sf} is increased. This parameter directly affects the transverse and longitudinal cross-sectional area of the substrate, and therefore, the resulting thermal resistance to heat flow. Unlike the previous case shown in Fig. 7(*a*), for higher values of δ_{sf}, there is less appreciable change in the overall thermal resistance between the vertical and horizontal sections of the fluid–solid interface. So, in Fig. 7(*b*), the heat flux through the vertical interfaces (AB and CD) is not maximum for the case of highest k_{sf}, rather it is maximum corresponding to some intermediate value of k_{sf}. This intermediate value of k_{sf} corresponds to that given in Fig. 6, at which $\overline{Nu}$ is maximum. Another noticeable effect is the change in the nature of heat flux near the corners B and C, with varying k_{sf}. The

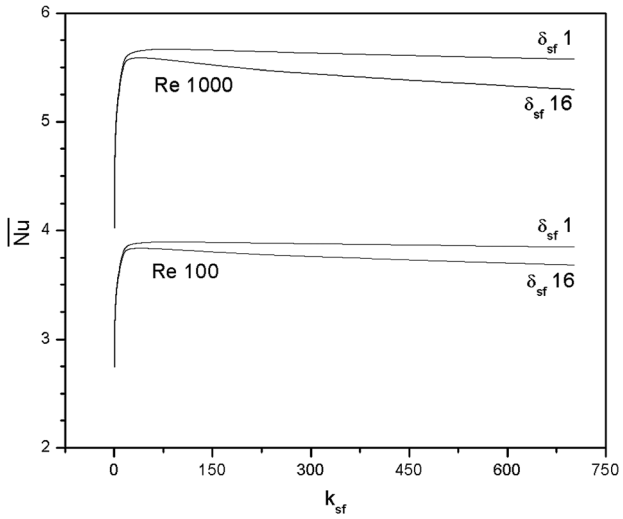

Fig. 6 Variation of average Nusselt number of the square microchannel as a function of conductivity ratio, k_{sf}; the thickness ratio (δ_{sf}) and flow condition (Re) are varied

local heat flux passing through the corners drastically increase with decreasing k_{sf}, asymptomatically approaching nullity for very high k_{sf}, and vice versa. This trend is clear from Fig. 7(*c*),

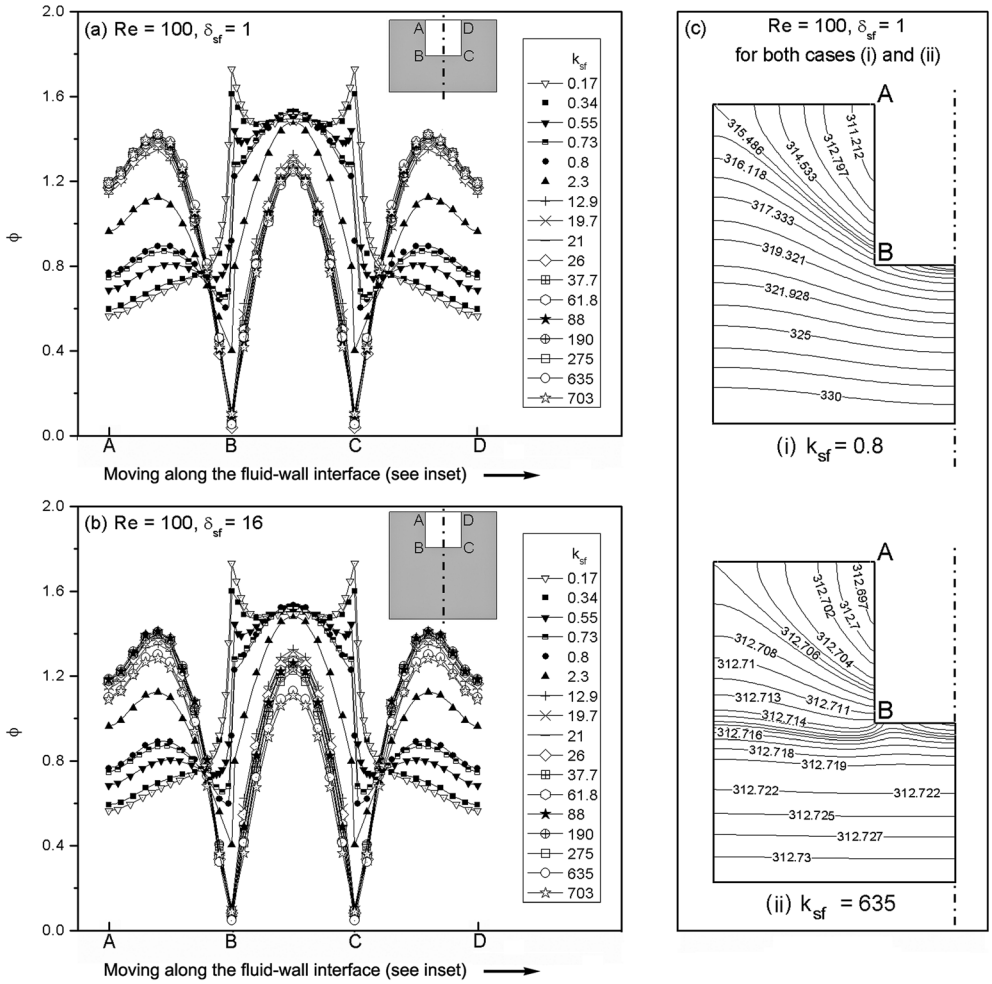

Fig. 7 Peripheral variation of dimensionless heat flux at a section in X-Y plane, midway along the length of the substrate (z = 60 mm or z* = 0.256) with varying conductivity ratio, k_{sf} when, (*a*) Re = 100, δ_{sf} = 1, (*b*) Re = 100, δ_{sf} = 16, and (*c*) isotherms corresponding to Re = 100, δ_{sf} = 1, and (i) k_{sf} = 0.8 and (ii) k_{sf} = 635

where the isotherms inside the computational substrate domain on the same plane, corresponding to the case of Fig. 7(*a*), are shown, respectively, for (i) $k_{sf} = 0.8$ and (ii) $k_{sf} = 635$. The shift in the local heat flux value from local minima (for large k_{sf}) to local maxima (for small k_{sf}) at location B (and at C) is attributed to the interplay of local conductive resistance of the substrate to the convective resistance at the fluid solid boundary. This local minimum at the corners was also observed by Qu and Mudawar [38]. However, as their study was only limited to higher values of $k_{sf,}$ they did not report the entire nature of variation of local heat flux with $k_{sf,}$ as seen in Fig. 7(*a*) and 7(*b*). Qualitatively similar isotherms are also obtained for the case described in Fig. 7(*b*).

To further exemplify the axial movement of heat in the substrate, the isotherms on the vertical plane of symmetry on Y-Z plane (see Fig. 1(*d*)), both in the fluid and solid domains, at $Re = 100$ and $\delta_{sf} = 1$ and 16, are shown in Fig. 8(*a*) and 8(*b*), respectively. For these two cases, $k_{sf} = 88.5$ (when $\delta_{sf} = 1$) and $k_{sf} = 37.7$ (when $\delta_{sf} = 16$), corresponds to maximum Nu, respectively. Low Re (= 100) is selected as representative case for highlighting higher effect of axial conduction in the substrate. Heat flux lines being orthogonal, these isotherms clearly indicate the impact of higher k_{sf} on axial conduction. For a given value of k_{sf}, the isotherm patterns in the solid domain are qualitatively similar for both $\delta_{sf} = 1$ and 16. The isotherms in the liquid domain highlight the fact that heat transport behavior at very low k_{sf}, is distinctly different from its higher valued counterparts. Second, the influence of δ_{sf} is also negligible on the temperature contours in the fluid domain. For these simulations, the inlet fluid temperature was maintained at 300 K and a constant heat input flux of 1.8 W/cm^2 has been applied.

The occurrence of a maximum Nusselt number was also checked for a microtube of circular cross section. Unlike channels cut on flat substrates, microtubes have radial symmetry. In addition, δ_{sf} can be increased by increasing the outer diameter of the tube, which increases the area of cross section by an order of square of the diameter. The variation of average Nusselt number with k_{sf}, at different flow Re and δ_{sf} (in this case, δ_{sf} is interpreted as the ratio of tube wall thickness to the inner radius) in a microtube of internal diameter 400 μm, is presented in Fig. 9. The tubular cross section essentially indicates similar qualitative variation of average Nusselt number, as noted for channel in a flat substrate in Fig. 6. Of course, in the case of the circular microtube $\delta_{sf} = 16$ leads to a much larger cross-sectional area of the substrate in the radial direction. Thus, for a circular tube too there lies an optimum value of k_{sf}, corresponding to which the average Nusselt number is maximum, for a given Re and δ_{sf}.

Recently, Kosar [25] investigated conjugate heat transfer on geometry similar to the present study. Very low thermal conductivity materials like polymide ($k_s = 0.25$, $k_{sf} = 0.409$), silica glass ($k_s = 1.005$ and $k_{sf} = 1.64$), quartz ($k_s = 1.3$ and $k_{sf} = 2.13$) were considered. Their findings suggested that Nusselt number decreases with decreasing the thermal conductivity of the substrate. While this is certainly in line with the results discussed in Fig. 6, the conclusions are only partly correct; Kosar [25] did not

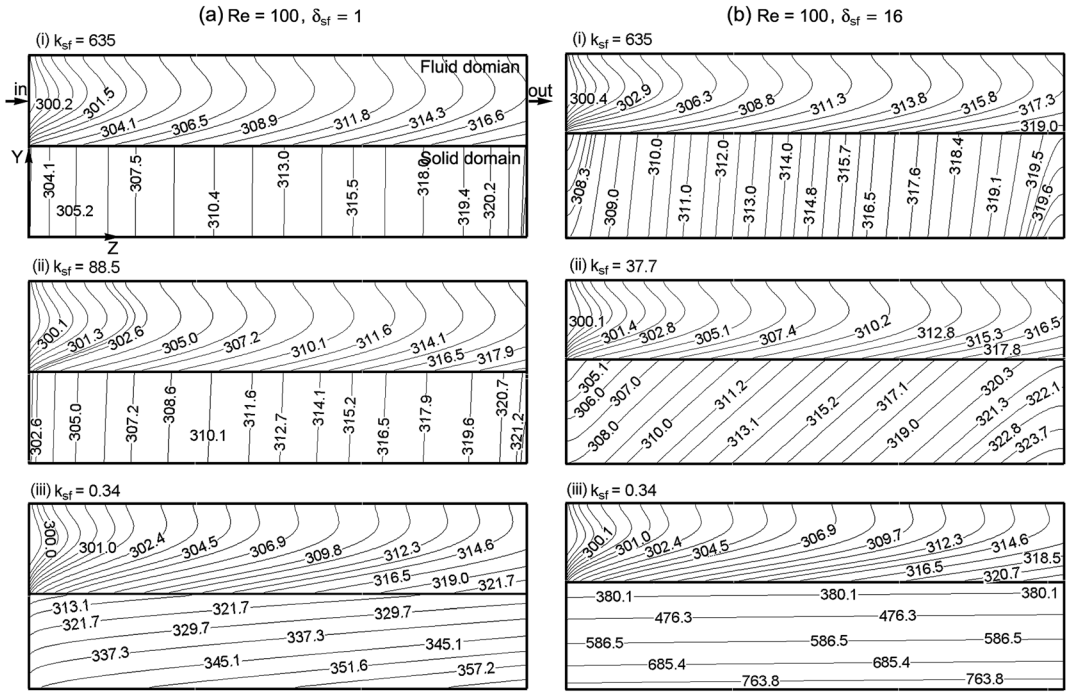

Fig. 8 Axial temperature distribution across the vertical plane of symmetry (Y-Z plane) showing isotherms in fluid and solid domain for different values of conductivity ratio, k_{sf} (*a*) Re = 100, δ_{sf} = 1, (*b*) Re = 100, δ_{sf} = 16. Detailing, as done in (*a*)–(*i*) is applicable to all figures

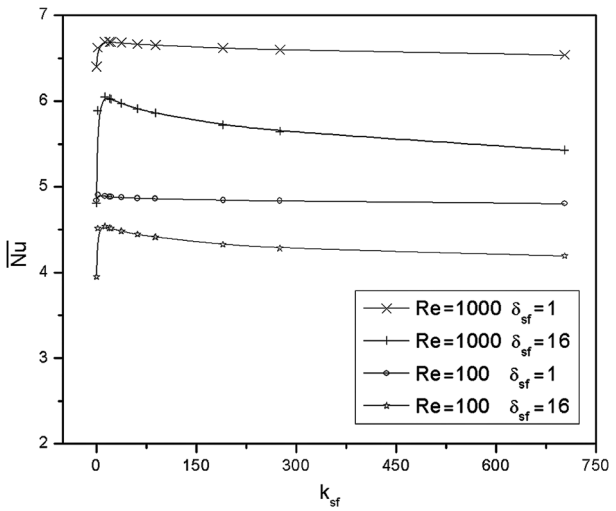

Fig. 9 Average Nusselt number of a circular microtube as a function of conductivity ratio k_{sf}; the thickness ratio (δ_{sf} = tube wall thickness/inner diameter) and flow condition (Re) are varied

capture the full spectrum of k_{sf} to get its optimum value. Similar study on conjugate effects on microtubes by Li et al. [13] also failed to capture the complete range of the effect of solid substrate on the variation of Nusselt number, as has been done in the present study.

4 Conclusions

A numerical study has been carried out to understand and highlight the effects of axial wall conduction in a conjugate heat transfer situation involving simultaneously developing laminar flow and heat transfer in a square microchannel machined on a flat substrate, with constant flux boundary condition imposed on bottom of the substrate wall. All the remaining walls of the substrate exposed to the surroundings are kept adiabatic. Simulations have been carried out for different ratios of wall to fluid conductivity ratio ($k_{sf} \sim 0.17$–703), substrate thickness to channel depth ($\delta_{sf} \sim 1$–24), and flow rate (Re $\sim$ 100–1000).

The results clearly show that, for a given flow rate and δ_{sf}, the thermal conductivity ratio k_{sf} is the key factor in determining the effects of axial wall conduction on the heat transport behavior. Higher k_{sf} leads to axial back conduction, thus decreasing the average Nusselt number as compared to the Nusselt number obtained for the case when the wall thickness is negligible. Very low k_{sf} leads to a situation where the channel heat transfer can be compared to a channel having zero wall thickness with only one side heated with a constant heat flux and the rest of the three sides being adiabatic; this leads to lower average Nusselt number. The results explicitly indicate the existence of an optimum value of the thermal conductivity ratio for maximizing the average Nusselt number, for a given flow rate and wall thickness ratio. It has also been shown that similar phenomena will be observed in substrates having a tubular geometry.

Acknowledgment

This work is funded by the Department of Science and Technology, Government of India, under the IIT Kanpur sponsored Project No: DST/CHE/20060304, titled "Micro-devices for Process Applications."

Nomenclature

A = cross-sectional area (m^2)
A_{sf} = ratio of cross-sectional area of solid substrate to channel (A_s/A_f)
Bi = Biot Number, as defined in Eq. (2)
c_p = specific heat (J/kg K)
d = diameter of circular tube (m)
D_h = hydraulic diameter (m)
h_z = local heat transfer coefficient (W/m^2 K)
k = thermal conductivity (W/m K)

k_{sf} = wall to fluid thermal conductivity ratio (k_s/k_f)
L = length of the channel (m)
M = axial conduction number
$\dot{m}$ = mass flow rate (kg/s)
NTU = number of transfer units
Nu = Nusselt number ($h \cdot D_h/k_f$)
$\overline{Nu}$ = average Nusselt number, as defined in Eq. (16)
P = parameter for axial conduction, as in Eqs. (5)–(8)
Pe = Peclet number (Re·Pr)
Pr = Prandtl number ($c_p \cdot \mu/k_f$)
q' = heat flux applied at the bottom of the substrate (W/m^2)
$\overline{q'}$ = average heat flux experienced at the channel walls (W/m^2)
q'_z = averaged local heat flux at any axial location (W/m^2)
r = radius (m)
Re = Reynolds number ($\rho \cdot \bar{u} \cdot D_h/\mu$)
T = temperature (K)
$\bar{u}$ = average velocity of fluid in the channel (m/s^2)
z^* = nondimensional axial distance along the channel length (-)

Greek Symbols

δ = thickness (m)
δ_{sf} = ratio of substrate thickness to channel height (δ_s/δ_f)
ΔT = difference between temperature at inlet and outlet location (K)
Θ = nondimensional temperature, as defined in Eq. (14) (-)
λ = conduction parameter, as defined in Eq. (1)
μ = dynamic viscosity (Pa s)
ξ = length ratio as defined in Eq. (2)
ρ = density (kg/m^3)
ϕ = nondimensional heat flux ($\overline{q'_z}/\overline{q'}$)
ω = width (m)

Subscripts

cond = conductive
conv = convective
f = fluid
i = inlet condition, inner
o = outlet condition, outer
s = solid
w = wall surface
z = axial length along the channel

References

[1] Kakac, S., Vasiliev, L. L., Bayazitoglu, Y., and Yener, Y., eds., 2005, *Microscale Heat Transfer: Fundamentals and Applications*, Dordrecht, The Netherlands.
[2] Kandlikar, S. G., Garimella, S., Li, D., Colin, S., and King, M. R., 2006, *Heat Transfer and Fluid Flow in Minichannels and Microchannels*, Elsevier, London.
[3] Yarin, L. P., Mosyak, A., and Hetsroni, G., 2009, *Fluid Flow, Heat Transfer and Boiling in Micro-Channels*, Springer-Verlag, Berlin.
[4] Tiselj, I., Hetsroni, G., Mavko, B., Mosyak, A., Pogrebhyak, E., and Segal, Z., 2004, "Effect of Axial Conduction on the Heat Transfer in Micro-Channels," Int. J. Heat Mass Transfer, **47**(12–13), pp. 2551–2565.
[5] Gamrat, G., Marinet, M. F., and Asendrych, D., 2005, "Conduction and Entrance Effects on Laminar Liquid Flow and Heat Transfer in Rectangular Microchannels," Int. J. Heat Mass Transfer, **48**(14), pp. 2943–2954.
[6] Hetsroni, G., Mosyak, A., Pogrebnyak, E., and Yarin, L. P., 2005, "Heat Transfer in Micro-Channels: Comparison of Experiments With Theory and Numerical Results," Int. J. Heat Mass Transfer, **48**(25–26), pp. 5580–5601.
[7] Sobierska, E., Kulenovic, R., Mertz, R., and Groll, M., 2006, "Experimental Results of Flow Boiling of Water in a Vertical Microchannel," Exp. Therm. Fluid Sci., **31**(2), pp. 111–119.
[8] Moharana, M. K, Agarwal, G., and Khandekar, S., 2011, "Axial Conduction in Single-Phase Simultaneously Developing Flow in a Rectangular Mini-Channel Array," Int. J. Therm. Sci., **50**(6), pp. 1001–1012.
[9] Bahnke, G. D., and Howard, C. P., 1964, "The Effect of Longitudinal Heat Conduction on Periodic-Flow Heat Exchanger Performance," ASME J. Eng. Power, **86**, pp. 105–120.
[10] Peterson, R. B., 1998, "Size Limits for Regenerative Heat Engines," Nanoscale Microscale Thermophys. Eng., **2**(2), pp. 121–131.
[11] Peterson, R. B., 1999, "Numerical Modeling of Conduction Effects in Microscale Counter Flow Heat Exchangers," Nanoscale Microscale Thermophys. Eng., **3**(1), pp. 17–30.
[12] Maranzana, G., Perry, I., and Maillet, D., 2004, "Mini- and Micro-Channels: Influence of Axial Conduction in the Walls," Int. J. Heat Mass Transfer, **47**(17–18), pp. 3993–4004.
[13] Li, Z., He, Y. L., Tang, G. H., and Tao, W. Q., 2007, "Experimental and Numerical Studies of Liquid Flow and Heat Transfer in Microtubes," Int. J. Heat Mass Transfer, **50**(17–18), pp. 3447–3460.
[14] Zhang, S. X., He, Y. L., Lauriat, G., and Tao, W. Q., 2010, "Numerical Studies of Simultaneously Developing Laminar Flow and Heat Transfer in Microtubes With Thick Wall and Constant Outside Wall Temperature," Int. J. Heat Mass Transfer, **53**(19–20), pp. 3977–3989.
[15] Petukhov, B. S., 1967, "Heat Transfer and Drag of Laminar Flow of Liquid in Pipes," Energiya, Moscow.
[16] Lelea, D., 2007, "The Conjugate Heat Transfer of the Partially Heated Microchannels," Heat Mass Transfer, **44**(1), pp. 33–41.
[17] Faghri, M., and Sparrow, E. M., 1980, "Simultaneous Wall and Fluid Axial Conduction in Laminar Pipe-Flow Heat Transfer," ASME Trans. J. Heat Transfer, **102**(1), pp. 58–63.
[18] Cotton, M. A., and Jackson, J. D., 1985, "The Effect of Heat Conduction in a Tube Wall Upon Forced Convection Heat Transfer in the Thermal Entry Region," *Numerical Methods in Thermal Problems*, Pineridge Press, Swansea, Vol. IV, pp. 504–515.
[19] Chiou, J. P., 1980, "The Advancement of Compact Heat Exchanger Theory Considering the Effects of Longitudinal Heat Conduction and Flow Nonuniformity," R. K. Shah, C. C. F. McDonald, P. Howard, eds., ASME-HTD Symposium on Compact Heat Exchangers, Vol. 10, pp. 101–121.
[20] Hessel, V., Renken, A., Schouten, J. C., and Yoshida, J. eds., 2009, *Micro Process Engineering: A Comprehensive Handbook, Volume 1: Fundamentals, Operations and Catalysis*, Wiley-VCH, Weinheim, Germnay.
[21] Cole, K. D., and Cetin, B., 2011, "The Effect of Axial Conduction on Heat Transfer in a Liquid Microchannel Flow," Int. J. Heat Mass Transfer, **54**(11–12), pp. 2542–2549.
[22] Guo, Z. Y., and Li, Z. X., 2003, "Size Effect on Single-Phase Channel Flow and Heat Transfer at Microscale," Int. J. Heat Fluid Flow, **24**(3), pp. 284–298.
[23] Lelea, D., 2009, "The Heat Transfer and Fluid Flow of a Partially Heated Microchannel Heat Sink," Int. Commun. Heat Mass Transfer, **36**(8), pp. 794–798.
[24] Nonino, C., Savino, S., Giudice, S. D., and Mansutti, L., 2009, "Conjugate Forced Convection and Heat Conduction in Circular Microchannels," Int. J. Heat Fluid Flow, **30**(5), pp. 823–830.
[25] Kosar, A., 2010, "Effect of Substrate Thickness and Material on Heat Transfer in Microchannel Heat Sinks," Int. J. Therm. Sci., **49**(4), pp. 635–642.
[26] Celata, G. P., Cumo, M., Marconi, V., McPhail, S. J., and Zummo, G., 2006, "Microtube Liquid Single-Phase Heat Transfer in Laminar Flow," Int. J. Heat Mass Transfer, **49**(19–20), pp. 3538–3546.
[27] Liu, Z., Zhao, Y., and Takei, M., 2007, "Experimental Study on Axial Wall Heat Conduction for Conductive Heat Transfer in Stainless Steel Microtube," Heat Mass Transfer, **43**(6), pp. 587–594.
[28] Moharana, M. K., Peela, N. R., Khandekar, S., and Kunzru, D., 2011, "Distributed Hydrogen Production From Ethanol in a Microfuel Processor: Issues and Challenges," Renewable Sustainable Energy Rev., **15**(1), pp. 524–533.
[29] Kolb, G., and Hessel, V., 2004, "Micro-Structured Reactors for Gas Phase Reactions," Chem. Eng. J., **98**(1–2), pp. 1–38.
[30] Xu, B., Ooi, K. T., Mavriplis, C., and Zaghloul, M. E., 2003, "Evaluation of Viscous Dissipation in Liquid Flow in Microchannels," J. Micromech. Microeng., **13**(1), pp. 53–57.
[31] Koo, J., and Kleinstreuer, C., 2004, "Viscous Dissipation Effects in Microtubes and Microchannels," Int. J. Heat Mass Transfer, **47**(14–16), pp. 3159–3169.
[32] Morini, G. L., 2006, "Scaling Effects for Liquid Flows in Microchannels," Heat Transfer Eng., **27**(4), pp. 64–73.
[33] ANSYS-FLUENT® 12.0 Users Guide, Ansys Inc., USA.
[34] Muzychka, Y. S., and Yovanovich, M. M., 1998, "Modeling Nusselt Number for Thermally Developing Laminar Flow in Non-Circular Ducts," Proceedings of the 7th AIAA/ASME Joint Thermophysics and Heat Transfer Conference, Albuquerque, June 14–18, Paper No. 98-2586.
[35] Muzychka, Y. S., and Yovanovich, M. M., 2004, "Laminar Forced Convection Heat Transfer in the Combined Entry Region of Non-Circular Ducts," ASME Trans. J. Heat Transfer, **126**(1), pp. 54–61.
[36] Lee, P. S., and Garimella, S. V., 2006, "Thermally Developing Flow and Heat Transfer in Rectangular Microchannels of Different Aspect Ratios," Int. J. Heat Mass Transfer, **49**(19–20), pp. 3060–3067.
[37] Shah, R. K., and London, A. L., 1978, Laminar Flow Forced Convection in Ducts (Advances in Heat Transfer), Academic Press, New York.
[38] Qu, W., and Mudawar, I., 2002, "Analysis of Three-Dimensional Heat Transfer in Micro-Channel Heat Sinks," Int. J. Heat Mass Transfer, **45**(19), pp. 3973–3985.